Muonic Atoms. I. Dynamic Hyperfine Structure in the Spectra of Deformed Nuclei*

D. HITLIN,† S. BERNOW, S. DEVONS, I. DUERDOTH,‡ J. W. KAST, E. R. MACAGNO, J. RAINWATER, AND C. S. WU
Department of Physics, Columbia University, New York, New York 10027
AND
R. C. BARRETT
University of Surrey, Guidford, United Kingdom

(Received 10 November 1969)

Precise measurements, using a stable high-resolution Ge(Li) spectrometer, have been made of the $K(2p\text{-}1s)$ and $L(3d\text{-}2p)$ muonic x-ray spectra for nine deformed even-even nuclei: ^{150}Nd, ^{152}Sm, ^{162}Dy, ^{164}Dy, ^{168}Er, ^{170}Er, ^{182}W, ^{184}W, and ^{186}W. From these measurements, parameters describing the nuclear charge distribution have been determined. Nuclear-polarization corrections have been included in the analysis. The accuracy of the determination of the parameters of the nuclear charge distribution is limited by theoretical rather than experimental uncertainties. Isotope shifts have been determined and compared with optical and electronic x-ray results.

I. INTRODUCTION

RECENT improvements in resolution and accuracy of the measurement of muonic x rays have made it possible to obtain new characteristics of the charge distribution of nuclei and to study the magnetic dipole and electric quadrupole form factors. This work is concerned with the quadrupole interaction. The measurements were begun in 1965 and additional experiments were carried out in 1966 and 1967. The earlier results and preliminary interpretations have been reported previously.[1–4] Similar results have been presented by the CERN group for a large number of deformed nuclei,[5] by Anderson *et al.*[6] for $^{238}_{92}$U and $^{232}_{90}$Th and by Coté *et al.*[7] for $^{238}_{92}$U and $^{232}_{90}$Th and several rare-earth nuclei.[8]

Wheeler,[9] in 1953, discussed in detail the static quadrupole interaction between the muon and nucleus and the resulting hyperfine structure in the $2p\rightarrow 1s$ muonic transition. The theory of dynamic quadrupole hyperfine structure was published by Wilets[10] and independently by Jacobson.[11] In the rare-earth region the interaction is so strong that second-order effects are important and a nucleus of zero ground-state spin has an observable hyperfine structure in the $3d$ and $2p$ muonic levels. We have analyzed the spectra in terms of a deformed Fermi distribution and found parameters which enable us to reproduce the spectra. We have assumed that the nuclei can be described by a simple rotational model and investigated to what extent we can test deviations from this model. The theoretical calculations have taken into account vacuum polarization, self-energy corrections, and nuclear polarization and dispersion corrections. At present the uncertainty in the nuclear polarization corrections is larger than the experimental errors.

II. THEORY

A. Energies

The Hamiltonian for the muon-nucleus system may be written as $H=H_\mu+H_N+H_{\rm INT}$, where H_μ is the Dirac Hamiltonian for a muon in a central field $V_0(r_\mu)$, H_N is the nuclear Hamiltonian and $H_{\rm INT}$ the remainder of the muon-nucleus interaction $\mathcal{V}$ which is given by

$$\mathcal{V}=-e^2\sum_{i=1}^{Z}(1/|\mathbf{r}_\mu-\mathbf{r}_i|^2).$$

Initially, we approximate $\mathcal{V}$ by V, the potential due to a static charge $\rho(\mathbf{r})$

$$V=-e^2\int[\rho(\mathbf{r})/|\mathbf{r}_\mu-\mathbf{r}|]d^3r,$$

* Work supported in part by the U.S. Atomic Energy Commission and the National Science Foundation.

† Present address: SLAC, Stanford, California.
‡ Present address: Physical Laboratory, The University, Manchester, England.

[1] D. Hitlin *et al.*, Bull. Am. Phys. Soc. **11**, 130 (1966); **12**, 75 (1967).
[2] C. S. Wu, in *Proceedings of the International Physics Conference, Gatlinburg, Tenn. 1966*, edited by R. L. Becker and A. Zucher (Academic Press Inc., New York, 1967); in *Proceedings of the International Conference on Hyperfine Structure and Nuclear Radiations, 1967*, edited by E. Matthias and D. A. Shirley (North-Holland Publishing Company, Amsterdam, 1967).
[3] D. Hitlin *et al.*, in *Proceedings of the International Conference on Electromagnetic Sizes of Nuclei, 1967* (Carleton University Press, Ottawa, Canada, 1967).
[4] S. Devons, also, K. Runge *et al.*, in *Proceedings of the International Conference on Intermediate Energy Physics, 1965* (The College of William and Mary Press, Williamsburg, Va., 1965).
[5] S. A. De Wit, G. Backenstoss, C. Daum, J. C. Sens, and H. L. Acker, Nucl. Phys. **87**, 657 (1967).
[6] R. J. McKee, Phys. Rev. **180**, 1139 (1969).
[7] R. E. Cote, W. V. Prestwich, A. K. Gaigalas, S. Raboy, C. C. Trail, R. A. Carrigan, P. D. Gupta, R. B. Sutton, M. N. Suzuki, and A. C. Thompson, Phys. Rev. **179**, 1134 (1969).
[8] R. A. Carrigan, Jr., P. D. Gupta, R. B. Sutton, M. N. Suzuki, A. C. Thompson, R. E. Cote, M. V. Prestwich, A. K. Gaigalas, and S. Raboy, Phys. Rev. Letters **20**, 874 (1968). See, also, Ref. 33.
[9] J. A. Wheeler, Phys. Rev. **92**, 812 (1953).
[10] L. Wilets, Kgl. Danske Videnskab. Selskab, Mat.-Fys. Medd. **29**, No. 3 (1954).
[11] B. A. Jacobsohn, Phys. Rev. **96**, 1637 (1954).

and treat $\delta H=\mathcal{V}-V$ as a perturbation.[12] For convenience we make a multipole expansion of $\rho(\mathbf{r})$

$$\rho(\mathbf{r})=\rho_0(r)+\rho_2 Y_{20}(\theta,\varphi)+\cdots. \tag{1}$$

Then

$$V_0(r_\mu)=-4\pi e^2\left(r_\mu^{-1}\int_0^{r_\mu}\rho_0(r)r^2dr+\int_{r_\mu}^{\infty}\rho_0(r)rdr\right).$$

The most important part of $H_{\rm INT}$ is the static quadrupole interaction[10]

$$H_Q=-\tfrac{1}{2}e^2Q_0 f(r_\mu)P_2(\cos\hat{\mu}\hat{N}), \tag{2}$$

where

$$Q_0 f(r_\mu)=\left(\frac{16\pi}{5}\right)^{1/2}\left(\frac{1}{r_\mu^3}\int_0^{r_\mu}\rho_2(r')r'^4dr' +r_\mu^2\int_{r_\mu}^{\infty}\rho(r')\frac{1}{r'}dr'\right)\to Q_0/r_\mu^3 \quad \text{as} \quad r_\mu\to\infty. \tag{3}$$

In analyzing muonic hyperfine spectra it has been customary to diagonalize H_Q in a basis (which we shall call the "model space") consisting of a spin doublet (e.g., $2p_{1/2}$, $2p_{3/2}$) and the nuclear ground-state rotational band. Chen has shown[13] that neglecting muon and nuclear states outside of the model space causes an error of several keV in the energy levels of ^{238}U. This result is confirmed by a coupled-channel calculation of McKinley.[14] Recently, Chen[13] has developed a method of simulating the admixture of higher states by using an effective interaction $H_{\rm eff}$, which contains the second-order terms connecting states inside the model space with those outside.

Within the model space, the matrix elements are of the form

$$\langle I_1Kl_1j_1;FM\mid H_Q\mid I_2Kl_2j_2;FM\rangle =\alpha_{j_1j_2}A_2(I_1l_1j_1I_2l_2j_2;KF),$$

where

$$\alpha_{j_1j_2}=-\tfrac{1}{10}Q_0e^2R(I_1I_2)\int(F_{j1}F_{j2}+G_{j1}G_{j2})f(r)\,dr \tag{4}$$

contains the nuclear structure dependence. Here the functions F_j/r and G_j/r are the large and small radial components of the Dirac wave function, and

$$R(I_1,I_2)=(\tfrac{4}{5}\pi)^{1/2}\langle I_1K\,||\,r^2Y_2\,||\,I_2K\rangle/(I_1K20\mid I_2K)Q_0 \tag{5}$$

is equal to unity in the limit of the rotational model.[15,16] The angular momentum factors are contained in the factor A_2 which is given by

$$A_2(I_1l_1j_1I_2l_2j_2KF)=(-1)^{F+I_2+j_1-j_2-(1/2)} \times 5[(2I_2+1)(2j_1+1)(2j_2+1)]^{1/2}(j_1-\tfrac{1}{2}j_2\tfrac{1}{2}\mid 20) \times(20I_2K\mid I_1K)W(I_1I_2j_1j_2;2F). \tag{6}$$

The notation of Edmonds[17] is used in the above.

The details of the calculation of $H_{\rm eff}$ are given in an accompanying paper by Chen.[13] For a given deformation, $H_{\rm eff}$ gives effective quadrupole matrix elements about 5% larger in the $2p$ states and 2% larger in the $3d$ states than the conventional calculation, about 2 and 0.1 keV, respectively. The corrections to the $1s$ binding energies owing to the mixing of higher states are shown in Table I.

TABLE I. Nuclear-polarization corrections to the $1s_{1/2}$ muonic levels of isotopes under study. Calculated by Chen (see preceding papers). The uncertainty is estimated to be about 15%.

Isotope	Nuclear polarization ($1s$ level) (keV)
^{150}Nd	6.87
^{152}Sm	8.05
^{162}Dy	9.90
^{164}Dy	10.34
^{168}Er	10.96
^{170}Er	10.39
^{182}W	9.43
^{184}W	9.01
^{186}W	8.95

B. Intensities

If we assume that the $4f$ states are statistically populated and neglect the quadrupole interaction in these states, we can calculate the relative intensities of the different lower transitions. We need consider only $E1$ transitions, since $E2$ and Auger transitions are very much slower.[18] In the $4f$ states the nucleus is in the ground state, $I=I_0$. The population of a particular $3d$ state, $|\alpha KF\rangle$, is then

$$P(\alpha,F)\propto(2F+1)\sum_j\langle I_0KjF\mid\alpha KF\rangle^2. \tag{7}$$

The amplitudes $\langle I_0KjF\mid\alpha KF\rangle$ are obtained when we diagonalize $H_{\rm eff}$ within our model space. The conventional method of obtaining the relative intensities is to evaluate

$$(E_i-E_f)^3\,|\,\langle I_fKj_fF_f\,||\,M(E_1)\,||\,I_fKj_fF_f\rangle\,|^2.$$

We have added correction terms which take account

[12] M. Y. Chen, second preceding paper, Phys. Rev. **C1**, 1167 (1970).
[13] M. Y. Chen, preceding paper, Phys. Rev. C **1**, 1176 (1970).
[14] J. M. McKinley, Phys. Rev. (to be published).
[15] A. Bohr and B. R. Mottelson, Kgl. Danske Videnskab. Selskab, Mat.-Fys. Medd. **27**, No. 16 (1953).
[16] A. Faessler and W. Greiner, Z. Physik **168**, 425 (1962).
[17] A. R. Edmonds, *Angular Momentum* (Princeton University Press, Princeton, N.J., 1957).
[18] D. West, Rept. Progr. Phys. **21**, 271 (1958).

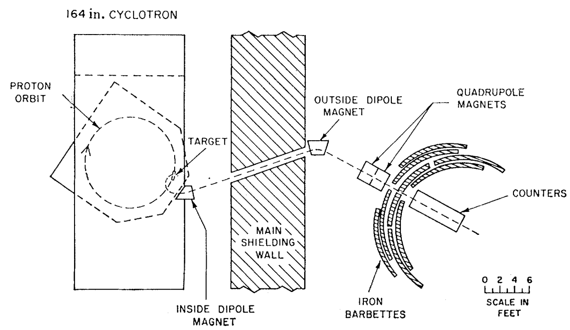

FIG. 1. Floor plan of the experimental arrangement.

of states outside our model space. The method of calculation of these terms is described in an accompanying paper by Chen.[13] These corrections change the relative intensities of the transitions by several percent.

C. Isomer Shift

When the muon cascades down to the $1s$ state, there is a substantial probability that the nucleus will be left in an excited state. In the presence of the $1s$ muon, the nuclear γ ray which is then emitted will differ in energy from the normal γ ray. This energy shift is due to the isomer shift or change in the size of the nucleus when excited, together with any difference in the nuclear polarization energies. Measurements of these shifts in deformed rare-earth nuclei have been presented by Columbia and CERN groups.[19–21]

If we consider two transitions from a single $2p$ state to $1s$ states with the nucleus in the ground state and 2^+ state, respectively, the difference ΔE will *not* be the same as that measured for the nuclear γ ray, but will be given by

$$\Delta E = E_{2+} + (\Delta E_{\text{isomer}}) + \Delta E_{\text{NS}},$$

where E_{2+} is the normal excitation energy of the 2^+ state, ΔE_{isomer} is the change in this excitation energy caused by the presence of the $1s$ muon (corrected for nonstatistical feeding and the fast radiationless $M1$ transition between the $F=\frac{5}{2}$ and $F=\frac{3}{2}$ states with $I=2$ and $j=\frac{1}{2}$). ΔE_{NS} is the shift in the center of gravity of the magnetic doublet due to the initial nonstatistical population.[22] If R_f is the ratio of the feeding of the $\frac{5}{2}$ and $\frac{3}{2}$ states then

$$\Delta E_{\text{NS}} = \Delta E_{\text{MAG}}[(R_F - \tfrac{3}{2})/\tfrac{5}{2}(1+R_F)],$$

where ΔE_{MAG} is the splitting between the $F=\frac{5}{2}$ and $F=\frac{3}{2}$ states.

D. Radiative Corrections

The most important correction to the Coulomb potential is that due to e^+e^- virtual pairs. The lowest-order term is[23,24]

$$V_{\text{vp}}(r) = \frac{4\alpha}{3\pi r}\int_0^\infty dr' [H(|r-r'|) - H(r,r')] r' \rho(r'),$$

where

$$H(r) = H(0) + r\{\ln(r\gamma/\lambda\!\!\!^{-}_e) - \tfrac{1}{6} - \tfrac{3}{8}\pi(\gamma/\lambda\!\!\!^{-}_e) + \tfrac{1}{2}(r/\lambda\!\!\!^{-}_e)^2 - \tfrac{1}{12}\pi(r/\lambda\!\!\!^{-}_e)^3 + O[(r/\lambda\!\!\!^{-}_e)^4 \ln(\gamma/\lambda\!\!\!^{-}_e)]\}.$$

Here $\ln\gamma = 0.557216$ is Euler's constant.

We neglect higher-order terms which we estimate to cause an error of less than 200 eV in the $1s$ state (Wickmann and Kroll).[25,26] We also neglect the quadrupole term in the vacuum polarization potential which would alter the quadrupole matrix elements in the $2p$ states by about 1%.[27]

The self-energy corrections to muon levels have been found to be important by Barrett *et al.*[28] The corrections are given by

$$E_{\text{LS}} = (\alpha/3\pi m^2)\langle\nabla^2 V\rangle[\ln(m/2\Delta E) + \tfrac{11}{24} + \tfrac{3}{8} - \tfrac{1}{5}] + (\alpha/8\pi m^2)\langle(2/r)(dV/dr)\boldsymbol{\sigma}\cdot\mathbf{L}\rangle,$$

where ΔE is the average excitation energy. We have obtained values of E_{LS} from the calculations of Barrett.[28]

III. EXPERIMENTAL PROCEDURE

A negative muon beam from the Nevis 160-in. 385-MeV synchron-cyclotron was produced, moderated,

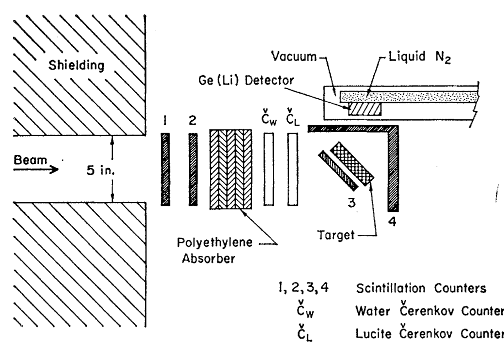

FIG 2. Schematic diagram of beam telescope and Ge(Li) detector placement.

[19] S. Bernow, S. Devons, I. Duerdoth, D. Hitlin, J. W. Kast, E. R. Macagno, J. Rainwater, K. Runge, and C. S. Wu, Phys. Rev. Letters **18**, 787 (1967).
[20] S. Bernow, S. Devons, I. Duerdoth, D. Hitlin, J. W. Kast, W. Y. Lee, E. R. Macagno, J. Rainwater, and C. S. Wu, Phys. Rev. Letters **21**, 457 (1968).
[21] R. Baader, H. Backe, R. Engfer, K. Hesse, E. Kankeleit, U. Schröder, H. K. Walter, and K. Wien, Phys. Letters **27B**, 425 (1968).
[22] A. Gal, L. Grodzins, and J. Hufner, Phys. Rev. Letters **21**, 453 (1968); H. Daniel, Naturwiss. **55**, 339 (1968).

[23] D. L. Hill and K. W. Ford, Phys. Rev. **94**, 1617 (1954).
[24] R. C. Barret, S. Brodsky, G. Erickson, and M. Goldhaber, Phys. Rev. **166**, 1589 (1968).
[25] E. Wickmann and N. Kroll, Phys. Rev. **101**, 843 (1956).
[26] C. S. Wu and L. Wilets, Ann. Rev. Nucl. Sci. **19**, 527 (1969).
[27] J. M. Pearson, Nucl. Phys. **45**, 401 (1963).
[28] R. C. Barrett, Phys. Letters **26B**, 93 (1968).

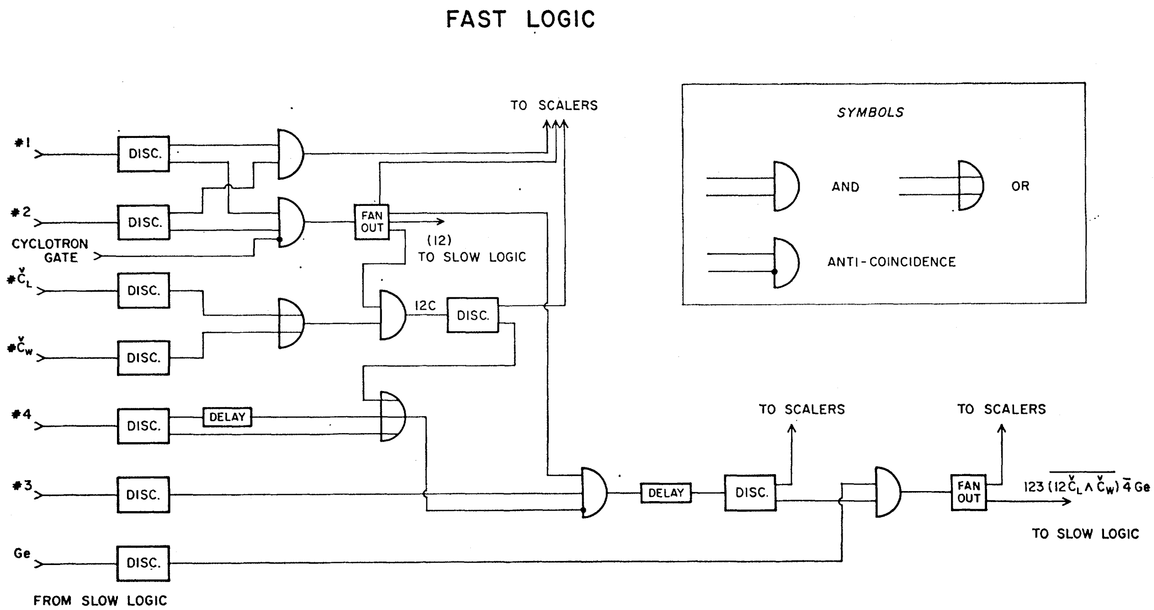

FIG. 3. Block diagram of the "fast logic," or beam telescope circuitry.

and stopped in the conventional manner.[29] Figure 1 is a floor plan of the beam transport system. The muon beam was extracted by the "inside dipole" magnet placed within the main shielding wall in the fringing field of the cyclotron magnet. The beam was then bent through approximately 45° by the "outside dipole" magnet for momentum selection, passed through a pair of quadrupoles focused on our targets and entered the experimental area, which was shielded by several thick steel barbettes and by lead bricks.

The beam telescope (Fig. 2) counters 1, 2, $\check{C}_L$, $\check{C}_W$, 3, and 4 defined a stopping muon. Most of the pions were stopped in the several inches of polyethylene absorber placed downstream from the 2 counter. Two Čerenkov counters, one of lucite ($\check{C}_L$) and one of water ($\check{C}_W$) were placed downstream from the absorber to discriminate against electrons, which, on account of their greater range, were not stopped but could be scattered into the Ge(Li) detector. The beam momentum was selected at (150 MeV/c). The index of refraction of the Čerenkov counters was chosen so that the electrons produced Čerenkov light, while the muons did not. Any particle which produced a count in the Čerenkov counter was vetoed. The 3 counter ($2\frac{1}{2}$ in.$\times 2\frac{1}{2}$ in.$\times\frac{1}{8}$ in.) had the same area as the targets, and thus signaled the entrance of a particle into the target. If a muon stopped in the target, it did not produce a count in the No. 4 counter. Thus a "muon stop" had the signature $123{\sim}(\check{C}_L$ or $\check{C}_W)4$, where $\sim$ stands for not. We were able to stop approximately 20 muons/sec per gram of target.

The beam telescope logic ("fast logic") is shown in Fig. 3. The "slow logic" is shown in Fig. 4. Pulses in the detector were amplified by a charge-sensitive preamplifier developed at the Pegram Electronics Laboratory.[30] The analog signal was then derived from a low-noise double RC shaped amplifier, also designed at Pegram.[31] A Miller-type baseline restorer was used to minimize counting-rate effects. A leading edge timing signal was derived from a tunnel diode discriminator set on the output of a fast amplifier connected to the detector preamplifier. The discriminator level was set typically at 100–150 keV. This signal was then placed in coincidence with the muon stop signal from the beam telescope.

The separated isotope targets were obtained on loan from Oak Ridge National Laboratory. They were all in the form of oxides, and were packaged in thin aluminum containers, with thin lucite faces for rigidity. Their dimensions were $2\frac{1}{2}$ in.$\times 2\frac{1}{2}$ in., with a thickness determined by the quantity of the isotope. The thickness varied from 0.5 gm/cm^2 for ^{152}Sm to 2.5 gm/cm^2 for most of the others. The actual weights and isotopic analysis of the targets are listed in Table II.

Muonic x rays produced by the muons stopped in the targets were detected by a 12-cc Ge(Li) detector made in our laboratories. The detector had a planar configuration with area 14 cm^2 and depletion depth of 8.5 mm. Its resolution was 4.0 keV at 1.33 MeV and 8.0 keV at 5.10 MeV.

[29] C. Nissim-Sabat, Ph.D. thesis, Columbia University, 1965 (unpublished); Nevis Laboratory Report No. 129, 1965 (unpublished).

[30] J. Hahn and T. Becker, Pegram Nuclear Physics Laboratories Annual Report No. NYO-GEN-72-132, 143, 1967 (unpublished).

[31] J. Hahn, A. Atzmon, and T. Becker, Pegram Nuclear Physics Laboratories Annual Report No. NYO-GEN-72-132, 143, 1967 (unpublished).

TABLE II. Weights and isotopic analysis of targets.

Isotope	Chemical form Sample No.	Weight	Isotopic analysis (%)	
^{150}Nd	No. 1357a		^{142}Nd	1.46
	Nd_2O_3	65.267 g	^{143}Nd	1.0
			^{144}Nd	1.52
			^{145}Nd	0.91
			^{146}Nd	1.51
			^{148}Nd	1.09
			^{150}Nd	92.5
^{152}Sm	No. 127401		^{147}Sm	0.08
	Sm_2O_3	23.016 g	^{148}Sm	0.07
			^{149}Sm	0.12
			^{150}Sm	0.1
			^{152}Sm	99.18
			^{154}Sm	0.45
	No. 81801		^{147}Sm	0.32
	Sm_2O_3	21.590 g	^{148}Sm	0.28
			^{149}Sm	0.51
			^{150}Sm	0.53
			^{152}Sm	91.43
			^{154}Sm	6.89
^{162}Dy	No. 122302		^{160}Dy	0.39
	Dy_2O_3	34.370 g	^{161}Dy	11.17
			^{162}Dy	82.1
			^{163}Dy	4.92
			^{164}Dy	1.39
	No. 122301		^{160}Dy	0.15
	Dy_2O_3	33.995 g	^{161}Dy	5.13
			^{162}Dy	91.04
			^{163}Dy	2.82
			^{164}Dy	0.86
^{164}Dy	No. 122502		^{161}Dy	1.05
	Dy_2O_3	57.214 g	^{162}Dy	3.18
			^{163}Dy	12.45
			^{164}Dy	83.23
	No. 122501		^{161}Dy	0.40
	Dy_2O_3	15.400 g	^{162}Dy	1.34
			^{163}Dy	5.55
			^{164}Dy	97.71
^{168}Er	No. 137502		^{166}Er	1.74
	Er_2O_3	95.793 g	^{167}Er	2.91
			^{168}Er	94.6
			^{170}Er	0.76
^{170}Er	No. 137601		^{166}Er	1.04
	Er_2O_3	120.860 g	^{167}Er	0.97
			^{168}Er	1.93
			^{170}Er	96.06
^{182}W	No. 128201		^{180}W	<0.05
	WO_3	128.834 g	^{182}W	94.4
			^{183}W	2.53
			^{184}W	2.32
			^{185}W	0.8
^{184}W	No. 128401		^{180}W	<0.05
	WO_3	162.681 g	^{182}W	1.91
			^{183}W	1.87
			^{184}W	94.3
			^{186}W	1.91
^{186}W	No. 128501		^{180}W	<0.03
	WO_3	128.499 g	^{182}W	0.38
			^{183}W	0.31
			^{184}W	2.05
			^{186}W	97.23

Pulses from the Ge(Li) detector were analyzed by a 4096-channel Victoreen ADC interfaced to an 8K PDP8 computer.[32] A block diagram of the ADC interface, the computer and its peripheral equipment appears in Fig. 5. The computer served as a control and central processor for peripheral equipment, and to service and stabilize the 4096-channel ADC. Since two 4096-channel spectra, one for muonic x rays and one for calibration, were to be recorded simultanously, and the PDP8 memory consists of only 8192 twelve-bit words, it was necessary to process and store the information from the ADC event by event on a magnetic tape. For this purpose, two 256-word buffers, one for each spectrum, were established in memory. When a buffer became full (that is, contained the

[32] V. Guiragossian, Pegram Nuclear Physics Laboratories Annual Report No. NYO-GEN-72-132, 165, 1967 (unpublished).

TABLE III. Energies of calibration γ rays.

Calibration energies Energy (keV)	Source	Ref.
511.006±0.005	Annihilation radiation	a
1173.226±0.040	^{60}Co	b
1274.52±0.10	^{22}Na	c
1332.483±0.046	^{60}Co	b
1368.53±0.04	^{24}Na	b
2753.92±0.12	^{24}Na	b
6129.96±0.46	^{16}N	d

[a] E. R. Cohen and J. W. M. DuMond, Rev. Mod. Phys. **37**, 537 (1963).
[b] G. Murray, R. L. Graham, and J. S. Geiger, Nucl. Phys. **63**, 353 (1965).
[c] W. W. Black and R. L. Heath, Nucl. Phys. **A90**, 650 (1967).
[d] C. Chasman, K. W. Jones, R. A. Ristinen, and D. E. Alburger, Phys. Rev. **159**, 830 (1967).

channel numbers of 256 events), its contents were written on magnetic tape along with a tag identifying the spectrum. A 4096-word section of memory was reserved for "live display" of either a portion of the spectra being taken, or the entire spectrum with channels summed. At the conclusion of a run, a second program was used to scan the magnetic tape to form histograms of the two types of events recorded thereon. These histograms were written on tape and drawn on a Calomp plotter so that immediate inspection of results was possible.

The low efficiency of the Ge(Li) detectors for high-energy γ rays, the relatively small number of stopped muons and the limited amounts of separated isotopes made it necessary to take data for some 8–12 h. In order to preserve the inherent resolution of the detectors, a computer-controlled stabilizing system was used to monitor and control the conversion gain and zero intercept of the ADC. A very stable (better than 50 ppm long-term stability over a range of 10°C in the ambient temperature, and 10% line voltage change) reference pulse generator operating at the cyclotron repetition rate of 70 Hz produced two reference pulses and two identification pulses.[33] The reference pulses were fed alternately to the input of the charge sensitive preamplifier along with the detector pulses, and were analyzed by the ADC. One pulse was centered at about channel 300 and the other at channel 4000. During a run, the computer checked the number of tagged pulser counts falling in bins of a preset number of channels on either side of the reference channels. The width of the bins depended on the amplifier gain and the detector resolution. Any drift in the system, whether it originated in the preamplifier, RC amplifier, or ADC would result in an unequal number of counts in adjacent bins. When the difference became greater than a preset number, a correction signal was generated and applied to the servostabilization controls for gain or zero correction. These controls consisted of dc stepping motors which drove two 10-turn Helipots connected to regulate the ramp discharge current for gain control and the base line voltage for zero control. The servostabilization was designed to apply the required number of 1/20 channel steps to restore the reference pulses to their proper channels. Pertinent information about the stabilization process, such as the total number of correction steps applied, the modulus of the number of steps, etc., was stored and could be typed out, so as to monitor the stability of the system during each run. With this method, the entire system was kept stable to less than 0.3 channels out of 4000 ($\sim$0.4 keV) over the duration of a run.

In order to be able to make a precise measurement

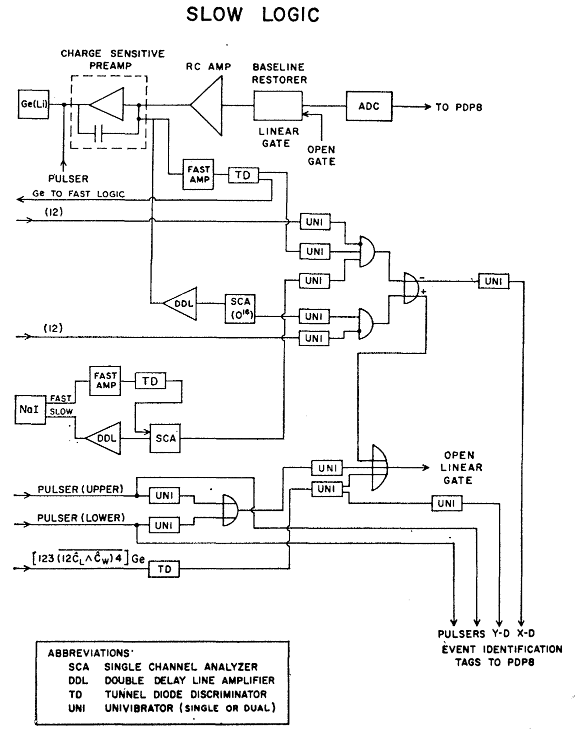

FIG. 4. Block diagram of the "slow logic": the detector circuitry, beam-detector coincidence logic, NaI(Tl)-Ge(Li) coincidence logic, and stabilization logic.

of the energies of the muonic x rays, calibration data were recorded simultaneously with the x-ray spectra. We chose calibration lines which, with one exception (the 6.130 line in ^{16}O from the β decay of ^{16}N) were part of a cascade which placed them in coincidence with a 1-MeV γ ray. These are listed in Table III. A calibration tag was generated by a coincidence between a $1\frac{1}{2}$ in.$\times 1\frac{1}{2}$ in. NaI(Tl) detector with a window set by a single-channel analyzer between 1.0 and 1.4 MeV, and the Ge(Li) detector. These coincidence pulses were used to gate the ADC and to identify the events as belonging to the calibration spectrum. The 6.130 line was produced in the usual way from the neutron reaction with the oxygen in a circulating-water target placed within the main shielding wall. This γ line was placed in self-coincidence, that is, the gating pulse was generated by the output of a single-channel analyzer with a window set on the double escape peak (5.108 MeV). This pulse was also identified and stored in the calibration spectrum. The use of pulser stabilization and simultaneous calibration meant that, in general, the quoted uncertainty in the energy of the muonic x rays was limited by the number of counts in the peaks or by uncertainties in the energy of the calibration γ rays, and not by drifts or broadening of lines as a result of the duration of individual runs.

[33] M. Konrad, Pegram Nuclear Physics Laboratories Annual Report No. NYO-GEN-72-132, 165, 1967 (unpublished).

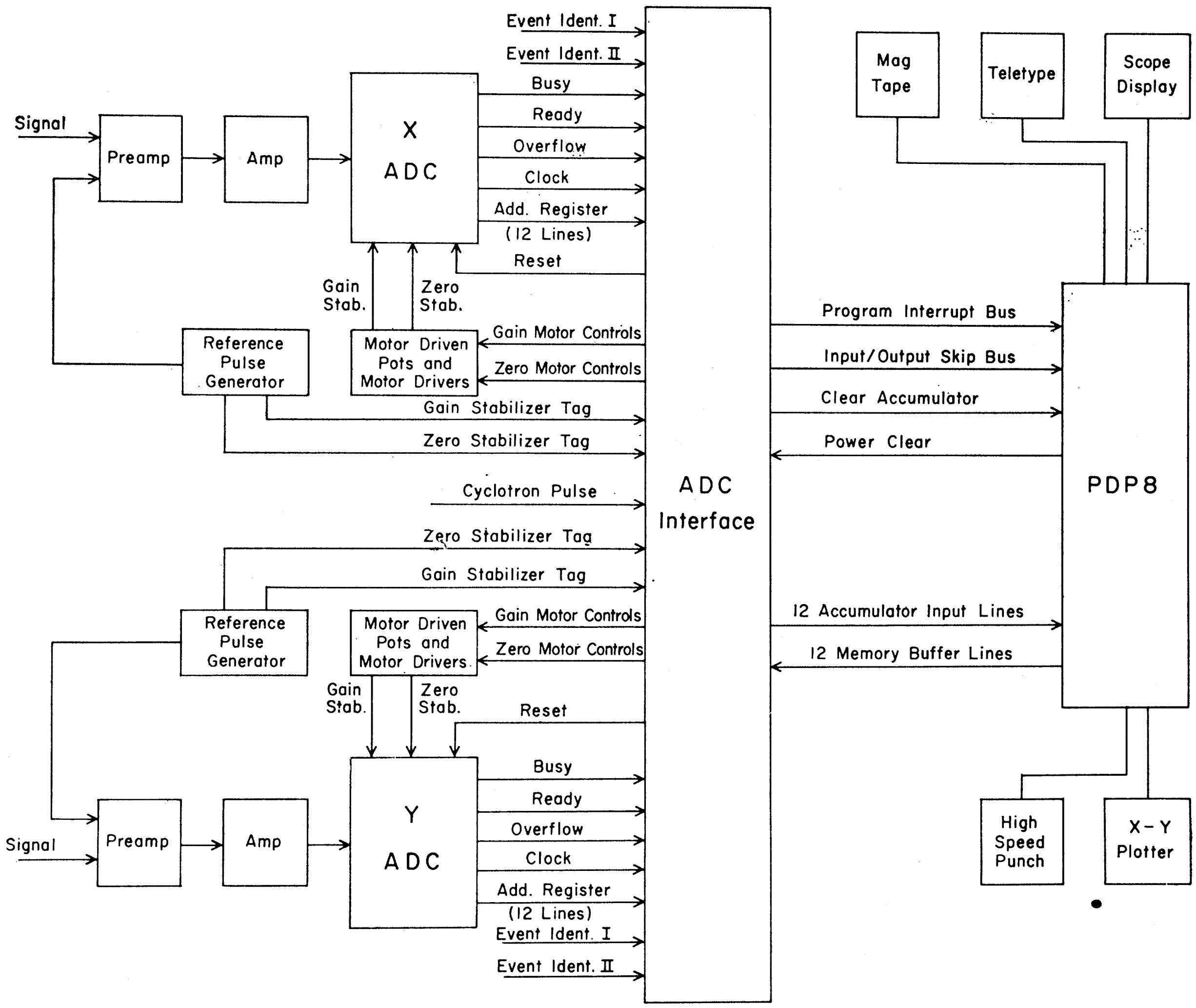

FIG. 5. Block diagram of interface to the PDP-8.

IV. DATA ANALYSIS

Each data run consisted of two 4096-channel spectra taken simultaneously. Several runs, of from 8- to 12-h duration were made for each target isotope. The position, area and FWHM for each significant peak in each of the spectra were determined by finding the best least-squares fit of a Gaussian to each peak (after background subtraction) by a χ^2 criterion. Background was subtracted by averaging several channels (usually 20) in either two or three regions adjoining the peaks of interest, and then fitting a straight line, parabola, Gaussian, or exponential curve through these points. The choice of the functional form for background subtractions was made by inspection. The quality of the Gaussian fit and the background subtraction could also be estimated by inspection of a graph, drawn by the computer, of the fitted curves superimposed on the data.

For a peak containing 1000 counts it was possible to determine the position to better than 0.5 keV. Some smaller peaks in individual runs contained less than 100 counts. The position of these peaks could be determined to approximately 1 keV.

An energy-versus-channel-number calibration curve was next obtained by finding the best least-squares fit of a quadratic to the channel numbers of the calibration lines of precisely known energy and assigning an energy-channel correspondence. The amplifier gain was set such that for all runs the slope was approximately 1.3 keV/channel. The quadratic nonlinearity amounted to a few channels out of 4096.

Once the positions of the various peaks were found, the corresponding energies were determined from the calibration curve. The energies quoted are the averaged result of several runs, with each determination weighted inversely as the square of the probable error. The relative intensities were found from the area

TABLE IV. Summary of parameters of deformed Fermi distribution which gave a best fit to the data. The distribution is given by $\rho(\mathbf{r}) = \rho_0\{1+\exp[((r-c(1+\beta Y_{20}))/a]\}^{-1}$. The quantity r_0 is defined by $c=r_0A^{1/3}$, while $t=(4\ln 3)a$. Both β(uniform), shown only for comparison, and $Q_{0\mathrm{CE}}(0,2)$ are derived from $B(E\colon 0^+\rightarrow 2^+)$ values given in Nucl. Data **1A**: 21 (1965), except for the tungsten isotopes, which are taken from Persson and Stokstad (Ref. 40).

Isotope	r_0	a	c	t	β	β (uniform)	$Q_{0\mathrm{CE}}$	$Q_{0\mu}$	χ^2/deg of freedom
$^{150}{}_{60}$Nd	1.105	0.533	5.87±0.03	2.34±0.06	0.278	0.279	5.17±0.12	5.15	35/14
$^{152}{}_{62}$Sm	1.106	0.538	5.90±0.03	2.36±0.05	0.296	0.304	5.85±0.15	5.78	31/14
$^{162}{}_{66}$Dy	1.102	0.547	6.01±0.03	2.40±0.05	0.338	0.334	7.12±0.12	7.36	25/14
$^{164}{}_{66}$Dy	1.116	0.499	6.11±0.03	2.19±0.06	0.334	0.347	7.50±0.20	7.42	21/14
$^{168}{}_{68}$Er	1.118	0.497	6.17±0.03	2.18±0.05	0.333	0.339	7.66±0.15	7.77	64/14
$^{170}{}_{68}$Er	1.132	0.442	6.27±0.03	1.94±0.05	0.326	0.329	7.45±0.13	7.75	22/14
$^{182}{}_{74}$W	1.131	0.482	6.41±0.02	2.12±0.05	0.248	0.252	6.58±0.06	6.57	11/14
$^{184}{}_{74}$W	1.128	0.493	6.42±0.02	2.17±0.05	0.237	0.236	6.21±0.06	6.27	12/10
$^{186}{}_{74}$W	1.132	0.478	6.46±0.02	2.10±0.05	0.222	0.224	5.93±0.05	5.90	29/14

under the Gaussians with background subtracted, as determined by the Gauss fit program. No corrections were made for isotopic impurities, since contributions from the impurities were generally smaller than the uncertainty in the background.

The peak-to-background ratios of the prominent lines are from 1.5:1 to 2.5:1 for most spectra, the ratio depending on the detector resolution for a given run. In the K x-ray double escape region, the background is due in part to Compton background from the full-energy peaks of the K x rays; in the L x-ray region, the background is due almost entirely to this cause. There is an additional source of background counts in the K x-ray region due to energy left in the Ge(Li) detector by minimum ionizing electrons in the beam which were not detected by the Čerenkov counters.

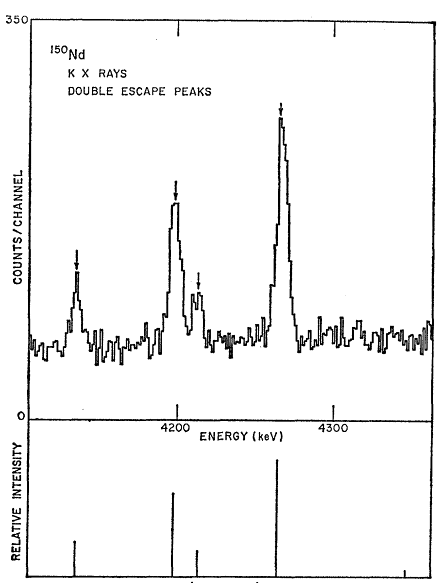

FIG. 6. K x rays of ^{150}Nb. A natural lanthanum target was also included as part of an isotope shift experiment (see Paper IV of this series). The most intense theoretical lines are shown beneath the experimental spectra. Lines which were compared with theory are indicated with an arrow (↓).

Our procedure has been to find the parameters of a function which we have termed a "deformed Fermi distribution" of the form

$$\rho(r,\theta) = \rho_0\{1+\exp[(r-c(1+\beta Y_{20})/a]\}^{-1}. \quad (8)$$

This distribution, which has also been used in the interpretation of electron scattering results,[34] is characterized by a half-density radius $c(1+\beta Y_{20})$ which varies with polar angle, but has a constant skin thickness $t(t=a\times 4\ln 3)$. It is a simple extension of the uniformly charged ellipsoid model.

There are two possibilities for determining the nuclear charge distribution. The first is to choose a distribution $\rho(\mathbf{r})$ and by a multipole expansion [Eq. (1)] calculate the monopole distribution (which determines the spherically symmetric potential $V(r)$ and thus the

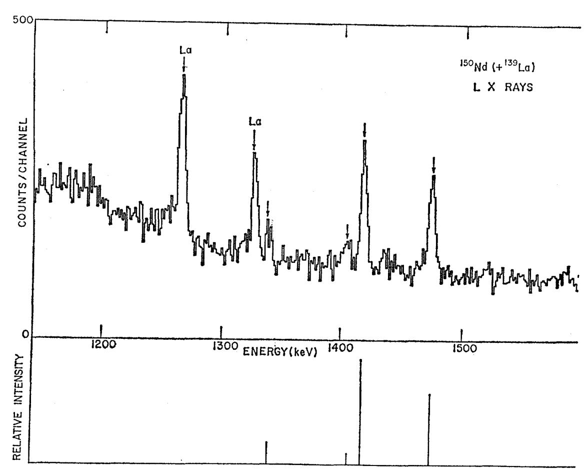

FIG. 7. L x rays of ^{150}Nd. Theoretical prediction shown underneath.

[34] G. J. C. Van Niftrik and R. Engfer, Phys. Letters **22**, 490 (1966).

TABLE V. Detailed summaries of analyses for individual nuclei. $E(I^+)$ is the energy of level of ground-state rotational band with spin I included in analysis. All energies are from *Nuclear Data Sheets* except for the 2^+ level of ^{150}Nd which was measured in our laboratory (Ref. 20). Parameters of deformed Fermi distribution as defined in the text. ρ_n is the central nucleon density on the assumption that proton and neutron densities are similar. $\langle r^2\rangle^{1/2}$ is the rms radius of the charge distribution. Unperturbed energy levels are calculated using potential derived from monopole charge distribution [Eq. (1)]. Unrenormalized quadrupole matrix elements are the $\alpha_{j_1j_2}$ defined by Eq. (6). These are the major contributors to $\langle H_{\rm eff}\rangle$ for the $2p$ and $3d$ states. Observed transitions—comparison of best-fit theoretical values of energies and relative intensities for those transitions identified in the K and L x-ray spectra. Intensities are normalized such that the sum of all observed transitions equals 100. A comparison of Coulomb excitation transition quadrupole moment with muonic x-ray best-fit value is also shown.

Isotope $^{150}{}_{60}$Nd

Energies of lowest rotational states (keV)

$E(2^+)=130.2$
$E(4^+)=397.$

Parameters of deformed Fermi distribution:

$r_0=1.105\pm0.005$ F	$c=5.871\pm0.027$ F
$a=0.533\pm0.013$ F	$t=2.342\pm0.057$ F
$\beta=0.278\pm0.003$	β (uniform) $=0.279$
$\rho_n=0.161$ F^{-3}	
$\langle r^2\rangle^{1/2}=5.048$ F	

Unperturbed energy levels (keV)	Quadrupole matrix elements (unrenormalized) (keV)
$1s_{1/2}=6820.468$	$2p$: $\alpha_{3/2,3/2}=24.63$
$2s_{1/2}=2099.791$	$\alpha_{3/2,1/2}=25.01$
$2p_{1/2}=2613.651$	$3d$: $\alpha_{5/2,5/2}=2.54$
$2p_{3/2}=2533.626$	$\alpha_{5/2,3/2}=2.56$
$3d_{3/2}=1147.034$	$\alpha_{3/2,3/2}=2.78$
$3d_{5/2}=1134.652$	

Observed transitions

	Energy (keV)		Intensity	
	Experiment	Theory	Experiment	Theory
K x rays	4135.96±0.41	4136.00	11.7±1.1	12.5
	4198.50±0.27	4198.39	31.3±1.2	33.4
	4212.81±0.49	4213.20	9.6±1.1	10.3
	4267.05±0.25	4266.88	47.4±1.2	43.9
L x rays	1341.00±0.64	1341.63	7.7±2.1	11.5
	1405.35±0.79	1406.44	9.6±1.8	5.2
	1419.01±0.17	1418.83	44.9±2.1	49.4
	1474.81±0.21	1474.93	37.8±2.1	33.9

$B(E2\text{: }0^+\to2^+)=(2.65\pm0.10)\times10^{-48}$ cm^4 e^2
$Q(0,2)_{\rm CE}=5.17\pm0.12$ b
$Q(0,2)_\mu=5.15\pm0.10$ b
$\chi^2=35$ for 14 deg of freedom

unperturbed energy levels and fine structure) and the quadrupole distribution (which determines the hyperfine splitting). This is the approach taken in the work presented here. The second possibility, discussed by Acker,[35] is to choose independent models of the $\rho_0(r)$

[35] H. L. Acker, Nucl. Phys. **87**, 153 (1966).

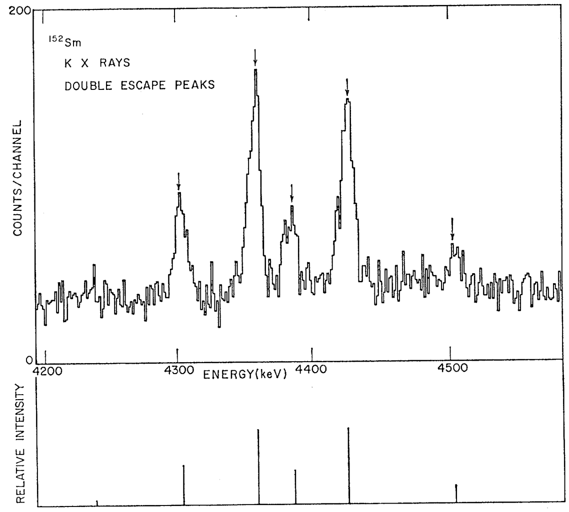

FIG. 8. K x rays of ^{152}Sm. Theoretical prediction shown underneath.

TABLE VI. Detailed summaries of analyses for individual nuclei. See caption of Table V.

Isotope $^{152}{}_{62}$Sm

Energies of lowest rotational states (keV)

$E(2^+)=121.78$
$E(4^+)=366.5$
$E(6^+)=712.$

Parameters of deformed Fermi distribution

$r_0=1.106\pm0.005$ F	$c=5.902\pm0.027$ F
$a=0.538\pm0.012$ F	$t=2.364\pm0.053$ F
$\beta=0.296\pm0.003$	β (uniform) $=0.304$
$\rho_n=0.160$ F^{-3}	
$\langle r^2\rangle^{1/2}=5.090$ F	

Unperturbed energy levels (keV)	Quadrupole matrix elements (unrenormalized) (keV)
$1s_{1/2}=7161.270$	$2p$: $\alpha_{3/2,3/2}=29.43$
$2s_{1/2}=2226.170$	$\alpha_{3/2,1/2}=29.86$
$2p_{1/2}=2790.117$	$3d$: $\alpha_{5/2,5/2}=3.13$
$2p_{3/2}=2701.846$	$\alpha_{5/2,3/2}=3.17$
$3d_{3/2}=1226.206$	$\alpha_{3/2,3/2}=3.45$
$3d_{5/2}=1212.086$	

Observed transitions

	Energy (keV)		Intensity	
	Experiment	Theory	Experiment	Theory
K x-rays	4304.62±0.55	4305.11	15.3±1.0	16.2
	4359.33±0.39	4359.19	32.4±1.0	32.0
	4385.17±0.66	4385.47	13.5±1.1	13.6
	4428.00±0.41	4427.57	32.6±1.0	31.5
	4506.77±1.05	4507.93	6.2±0.7	6.7
L x-rays	1441.27±0.37	1441.09	18.8±1.0	19.4
	1521.58±0.15	1521.45	40.3±1.7	45.0
	1575.34±0.23	1575.69	40.9±1.4	35.6

$B(E2\text{: }0^+\to2^+)=(3.40\pm0.12)\times10^{-48}$ cm^4 e^2
$Q(0,2)_{\rm CE}=5.85\pm0.15$ b
$Q(0,2)_\mu=5.78\pm0.10$ b
$\chi^2=31$ for 14 deg of freedom

and $\rho_2(r)$ distributions. Acker used a spherical Fermi distribution for $\rho_0(r)$ and a gaussian distribution for $\rho_2(r)$ to fit the ^{238}U muonic x-ray data of CERN. His conclusion was that the data were not sufficiently precise to allow determination of all five parameters necessary to specify the functions $\rho_0(r)$ and $\rho_2(r)$.

Even among those analyses which use a single distribution, there has been no general agreement on the best way to introduce a third (or a fourth) parameter. This has made comparison of the results of different laboratories difficult. For a discussion of the various distributions employed, see Devons and Duerdoth.[36]

If the rotational model holds exactly, then the ratio

$$R=Q_0(2,2)/Q_0(0,2)$$

will be exactly $+1$ for a prolate equilibrium shape and -1 for an oblate shape. Thus in this limit, the ratio of the matrix elements

$$\frac{Q_0(2,2)\langle nj_1 \mid f(r) \mid nj_2\rangle}{Q_0(0,2)\langle nj_1 \mid f(r) \mid nj_2\rangle}$$

will be ± 1. Any deviation from this value indicates a failure of the rotational model. We have investigated the sensitivity of the present data to such deviations by varying R about unity.

By choosing c, a, and β, we can calculate the entire muonic x-ray spectrum, including the muon energy levels in the monopole field of the nucleus and the hyperfine splitting. A search routine varies the three parameters c, a, and β in order to find a best fit to the experimentally measured quantities. The experimental quantities are (1) the hyperfine splittings of the K and L x rays, (2) the absolute energies of the K and L x rays, (3) the relative intensities of the components of the K and L x rays, and (4) the tran-

TABLE VII. Detailed summaries of analyses for individual nuclei. See caption of Table V.

Isotope $^{162}_{66}$Dy

Energies of lowest rotational states: (keV)
$E(2^+)=80.7$
$E(4^+)=265.9$
$E(6^+)=549.1$

Parameters of deformed Fermi distribution

$r_0=1.102\pm0.005$ F	$c=6.007\pm0.027$ F
$a=0.547\pm0.012$ F	$t=2.404\pm0.053$ F
$\beta=0.338\pm0.003$	β (uniform) $=0.334$
$\rho_n=0.161$ F^{-3}	
$\langle r^2\rangle^{1/2}=5.211$ F	

Unperturbed energy levels (keV)	Quadrupole matrix elements (unrenormalized) (keV)
$1s_{1/2}=7825.569$	$2p$: $\alpha_{3/2,3/2}=41.70$
$2s_{1/2}=2444.924$	$\alpha_{3/2,1/2}=42.19$
$2p_{1/2}=3156.318$	$3d$: $\alpha_{5/2,5/2}=4.77$
$2p_{3/2}=3051.117$	$\alpha_{5/2,3/2}=4.83$
$3d_{3/2}=1392.897$	$\alpha_{3/2,3/2}=5.29$
$3d_{5/2}=1374.778$	

Observed transitions

	Energy (keV) Experiment	Theory	Intensity Experiment	Theory
K x rays	4610.96±0.50	4610.60	18.0±1.7	19.4
	4643.55±0.40	4643.58	33.4±1.7	30.0
	4690.86±0.90	4691.31	6.9±1.5	11.0
	4722.46±0.95	4723.01	14.0±1.5	15.8
	4803.57±0.90	4803.71	27.7±2.1	23.8
L x rays	1646.98±0.30	1646.59	36.4±2.6	37.0
	1759.51±0.80	1758.99	26.5±3.5	27.4
	1789.13±0.75	1788.57	37.1±3.2	35.6

$B(E2:\ 0^+\to2^+)=(5.06\pm0.15)\times10^{-48}$ cm^4 e^2
$Q(0,2)_{CE}=7.12\pm0.15$ b
$Q(0,2)_\mu=7.36\pm0.10$ b
$\chi^2=25$ for 14 deg of freedom

TABLE VIII. Detailed summaries of analyses for individual nuclei. See caption of Table V.

Isotope $^{164}_{66}$Dy

Energies of lowest rotational states: (keV)
$E(2^+)=73.39$
$E(4^+)-242.33$
$E(6^+)=501.3$

Parameters of deformed Fermi distribution

$r_0=1.116\pm0.006$ F	$c=6.109\pm0.033$ F
$a=0.499\pm0.013$ F	$t=2.193\pm0.057$ F
$\beta=0.334\pm0.005$	β (uniform) $=0.347$
$\rho_n=0.157$ F^{-3}	
$\langle r^2\rangle^{1/2}=5.218$ F	

Unperturbed energy levels (keV)	Quadrupole matrix elements (unrenormalized) (keV)
$1s_{1/2}=7815.677$	$2p$: $\alpha_{3/2,3/2}=42.06$
$2s_{1/2}=2474.425$	$\alpha_{3/2,1/2}=42.54$
$2p_{1/2}=3156.186$	$3d$: $\alpha_{5/2,5/2}=4.84$
$2p_{3/2}=3051.222$	$\alpha_{5/2,3/2}=4.90$
$3d_{3/2}=1392.916$	$\alpha_{3/2,3/2}=5.37$
$3d_{5/2}=1374.796$	

Observed transitions

	Energy (keV) Experiment	Theory	Intensity Experiment	Theory
K x rays	4602.07±0.70	4602.20	15.6±1.4	19.4
	4632.61±0.50	4632.23	29.2±1.4	29.7
	4675.31±0.95	4675.59	10.1±1.0	9.8
	4717.37±0.90	4717.55	13.7±1.2	15.9
	4790.63±0.50	4790.94	28.2±1.4	25.1
L x rays	1649.37±0.40	1649.38	34.0±3.3	38.3
	1764.79±0.66	1764.73	27.0±2.8	26.1
	1790.08±0.46	1789.95	39.1±2.8	35.6

$B(E2:\ 0^+\to2^+)=(5.58\pm0.25)\times10^{-48}$ cm^4 e^2
$Q(0,2)_{CE}=7.50\pm0.20$ b
$Q(0,2)_\mu=7.42\pm0.10$ b
$\chi^2=21$ for 14 deg for freedom

[36] S. Devons and I. Duerdoth, Advances in Nuclear Physics (Plenum Publishing Corp., New York, 1969), Vol. 2.

TABLE IX. Detailed summaries of analyses for individual nuclei. See caption of Table V.

Isotope $^{168}{}_{68}$Er

Energies of lowest rotational states (keV)
$E(2^+)=79.8$
$E(4^+)=264.3$
$E(6^+)=548.9$

Parameters of deformed Fermi distribution

$r_0=1.118\pm0.005$ F	$c=6.169\pm0.028$ F
$a=0.497\pm0.012$ F	$t=2.184\pm0.053$ F
$\beta=0.333\pm0.003$	β (uniform) $=0.339$
$\rho_n=0.157$ F^{-3}	
$\langle r^2\rangle^{1/2}=5.260$ F	

Unperturbed energy levels (keV)	Quadrupole matrix elements (unrenormalized) (keV)
$1s_{1/2}=8156.900$	$2p$: $\alpha_{3/2,3/2}=46.37$
$2s_{1/2}=2605.926$	$\alpha_{3/2,1/2}=46.82$
$2p_{1/2}=3347.256$	$3d$: $\alpha_{5/2,5/2}=5.53$
$2p_{3/2}=3233.204$	$\alpha_{5/2,3/2}=5.60$
$3d_{3/2}=1480.457$	$\alpha_{3/2,3/2}=6.16$
$3d_{5/2}=1460.048$	

Observed transitions

	Energy (keV)		Intensity	
	Experiment	Theory	Experiment	Theory
K x rays	4746.24±0.50	4746.16	15.8±1.4	19.6
	4779.08±0.40	4779.26	38.6±1.8	29.6
	4826.38±0.80	4825.96	6.5±1.2	10.0
	4874.31±0.50	4873.20	12.2±1.2	15.8
	4952.36±0.40	4953.00	26.9±1.4	24.9
L x rays	1742.99±0.36	1743.17	37.9±2.3	37.9
	1870.51±0.82	1870.22	23.4±2.6	26.4
	1896.71±0.62	1896.48	38.7±3.3	35.6

$B(E2\colon 0^+\rightarrow2^+)=(5.80\pm0.20)\times10^{-48}$ cm^4 e^2
$Q(0,2)_{\rm CE}=7.66\pm0.15$ b
$Q(0,2)_\mu=7.77\pm0.10$ b
$\chi^2=64$ for 14 deg of freedom

sition moment $Q_0(0,2)$ as measured by Coulomb excitation experiments.

The search program calculates these quantities for specific values of the parameters of the charge distribution, computes the χ^2 of the fit

$$\chi^2=\sum_i\left[(\text{expt}_i-\text{theor}_i)^2/(\text{expt err}_i)^2\right]$$

and then varies the parameters in order to obtain a "best fit," i.e., the minimum χ^2. A few searches in which the ratio R was also allowed to vary from $+1$ were made in order to test the validity of the rotational model.

V. RESULTS AND DISCUSSION

The parameters of the deformed Fermi distribution which give a best fit to the data are summarized for the eight nuclei in Table IV. Details of the individual cases are given in Tables V–XIII. The K and L x-ray experimental spectra, together with the ten most prominent lines of the theoretical spectra are shown in Figs. 6–23.

The χ^2 quoted in the tables is the value obtained from fitting energies, HFS splittings, intensities, and the quadrupole moment. The worst fit is, invariably, that of the intensities. In the case of ^{168}Er, for example, out of a total $\chi^2=64$ for 14 deg of freedom, the fit to the intensities gives χ^2(intensities) $=55.0$, whereas the energies and splittings give only 8.5 and the quadrupole moment 0.5.

The errors quoted in the parameters of the distribution have two sources; uncertainty in the nuclear polarization and Lamb-shift corrections, and the sensitivity of χ^2 to the variation of the values of the parameters about those values which yield minimum χ^2. Uncertainties of the first type were accounted for by

TABLE X. Detailed summaries of analyses for individual nuclei. See caption of Table V.

Isotope $^{170}{}_{68}$Er

Energies of lowest rotational states (keV)
$E(2^+)=79.3$
$E(4^+)=261.$
$E(6^+)=542.$

Parameters of deformed Fermi distribution

$r_0=1.132\pm0.005$ F	$c=6.271\pm0.028$ F
$a=0.442\pm0.012$ F	$t=1.942\pm0.053$ F
$\beta=0.326\pm0.003$	β (uniform) $=0.329$
$\rho_n=0.153$ F^{-3}	
$\langle r^2\rangle^{1/2}=5.264$ F	

Unperturbed energy levels (keV)	Quadrupole matrix elements (unrenormalized) (keV)
$1s_{1/2}=8148.494$	$2p$: $\alpha_{3/2,3/2}=46.31$
$2s_{1/2}=2605.390$	$\alpha_{3/2,1/2}=46.76$
$2p_{1/2}=3347.428$	$3d$: $\alpha_{5/2,5/2}=5.55$
$2p_{3/2}=3233.550$	$\alpha_{5/2,3/2}=5.63$
$3d_{3/2}=1480.481$	$\alpha_{3/2,3/2}=6.19$
$3d_{5/2}=1460.069$	

Observed transitions

	Energy (keV)		Intensity	
	Experiment	Theory	Experiment	Theory
K x rays	4738.26±0.47	4738.13	18.1±0.8	19.7
	4771.37±0.50	4770.96	28.3±1.0	29.6
	4817.30±0.78	4817.43	8.7±1.0	10.0
	4864.99±0.50	4864.88	15.0±1.0	15.9
	4943.75±0.43	4944.18	25.7±1.3	24.8
L x rays	1743.45±0.30	1743.57	37.2±1.5	37.9
	1870.97±0.27	1870.32	26.9±1.8	26.5
	1895.89±0.24	1896.35	35.9±1.3	35.6

$B(E2\colon 0^+\rightarrow2^+)=(5.53\pm0.15)\times10^{-48}$ cm^4 e^2
$Q(0,2)_{\rm CE}=7.45\pm0.13$ b
$Q(0,2)_\mu=7.75\pm0.10$ b
$\chi^2=22$ for 14 deg of freedom

applying nuclear polarization and Lamb-shift corrections as large as the quoted value plus and minus the quoted uncertainty, and noting what parameter variations were produced. Uncertainties of the second type were found by calculating χ^2 as a function of small changes in a single parameter and all pairs of parameters about the values which yield the minimum χ^2. The resulting matrix is then inverted for these step sizes in the parameters. The step sizes are varied until those steps in each parameter are found which result in an increase of χ^2 of 1 after inversion. These uncertainties, amounting to one standard deviation, and including correlations, are then the diagonal elements of the inverse matrix. The two types of uncertainties are then combined in quadrature to arrive at the stated errors.

We found that uncertainties in the calculated Lamb shifts and nuclear polarization corrections limited the

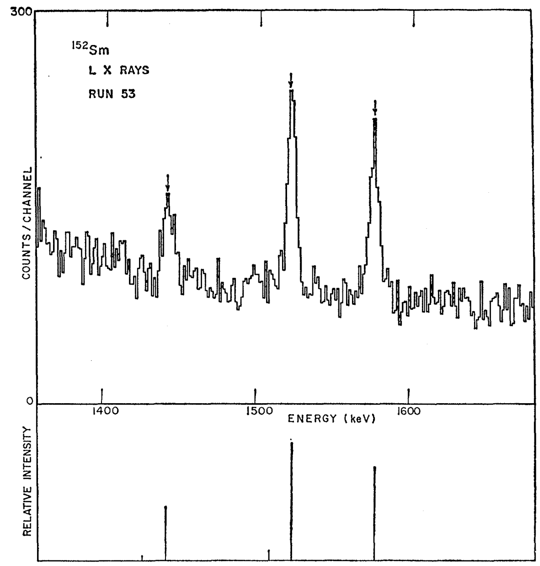

FIG 9. L x rays of ^{152}Sm. Theoretical prediction shown underneath.

TABLE XI. Detailed summaries of analyses for individual nuclei. See caption of Table V.

Isotope $^{182}{}_{74}$W

Energies of lowest rotational states (keV)

$E(2^+) = 100.07$
$E(4^+) = 329.42$
$E(6^+) = 680.4$

Parameters of deformed Fermi distribution

$r_0 = 1.131 \pm 0.004$ F	$c = 6.409 \pm 0.023$ F
$a = 0.482 \pm 0.012$ F	$t = 2.118 \pm 0.053$ F
$\beta = 0.248 \pm 0.002$	β (uniform) $= 0.252$
$\rho_n = 0.154$ F^{-3}	
$\langle r^2 \rangle^{1/2} = 5.357$ F	

Unperturbed energy levels (keV)	Quadrupole matrix elements (unrenormalized) (keV)
$1s_{1/2} = 9202.090$	$2p\alpha_{3/2,3/2} = 45.25$
$2s_{1/2} = 3017.098$	$\alpha_{3/2,1/2} = 45.49$
$2p_{1/2} = 3951.082$	$3d$: $\alpha_{5/2,5/2} = 5.97$
$2p_{3/2} = 3807.577$	$\alpha_{5/2,3/2} = 6.05$
$3d_{3/2} = 1760.080$	$\alpha_{3/2,3/2} = 6.74$
$3d_{5/2} = 1731.518$	

Observed transitions

	Energy (keV) Experiment	Energy (keV) Theory	Intensity Experiment	Intensity Theory
K x rays	5196.13 ± 0.50	5196.33	16.9 ± 0.8	17.6
	5227.96 ± 0.35	5227.63	31.0 ± 1.0	31.4
	5295.86 ± 0.90	5296.40	7.6 ± 0.6	8.2
	5319.70 ± 0.70	5319.51	16.0 ± 0.8	14.5
	5419.34 ± 0.40	5419.58	28.5 ± 1.0	28.3
L x rays	2050.30 ± 0.30	2050.32	41.9 ± 1.6	40.4
	2173.57 ± 0.50	2173.50	24.0 ± 1.3	23.3
	2213.69 ± 0.80	2213.68	34.1 ± 1.6	36.2

$B(E2\colon 0^+ \to 2^+) = (4.15 \pm 0.20) \times 10^{-48}$ cm^4 e^2
$Q(0,2)_{\mathrm{CE}} = 6.58 \pm 0.06$ b
$Q(0,2)_\mu = 6.57 \pm 0.08$ b
$\chi^2 = 11$ for 14 deg of freedom

TABLE XII. Detailed summaries of analyses for individual nuclei. See caption of Table V.

Isotope $^{184}{}_{74}$W

Energies of lowest rotational states (keV)

$E(2^+) = 111.12$
$E(4^+) = 364.0$
$E(6^+) = 748.2$

Parameters of deformed Fermi distribution

$r_0 = 1.128 \pm 0.004$ F	$c = 6.416 \pm 0.023$ F
$a = 0.493 \pm 0.012$ F	$t = 2.167 \pm 0.053$ F
$\beta = 0.237 \pm 0.002$	β (uniform) $= 0.236$
$\rho_n = 0.155$ F^{-3}	
$\langle r^2 \rangle^{1/2} = 5.369$ F	

Unperturbed energy levels (keV)	Quadrupole matrix elements (unrenormalized) (keV)
$1s_{1/2} = 9192.510$	$2p$: $\alpha_{3/2,3/2} = 43.11$
$2s_{1/2} = 3015.182$	$\alpha_{3/2,1/2} = 43.33$
$2p_{1/2} = 3949.961$	$3d$: $\alpha_{5/2,5/2} = 5.70$
$2p_{3/2} = 3806.796$	$\alpha_{5/2,3/2} = 5.78$
$3d_{3/2} = 1760.074$	$\alpha_{3/2,3/2} = 6.43$
$3d_{5/2} = 1731.521$	

Observed transitions

	Energy (keV) Experiment	Energy (keV) Theory	Intensity Experiment	Intensity Theory
K x rays	5188.15 ± 0.50	5188.25	21.2 ± 1.0	23.3
	5222.49 ± 0.30	5222.06	42.8 ± 1.2	41.9
	5413.59 ± 0.50	5413.26	36.0 ± 1.1	34.8
L x rays	2047.10 ± 0.60	2047.16	40.1 ± 1.3	38.9
	2161.25 ± 0.50	2161.05	24.2 ± 1.1	25.0
	2209.81 ± 0.60	2209.78	35.7 ± 1.3	36.1

$B(E2\colon 0^+ \to 2^+) = (3.66 \pm 0.15) \times 10^{-48}$ cm^4 e^2
$Q(0,2)_{\mathrm{CE}} = 6.21 \pm 0.06$ b
$Q(0,2)_\mu = 6.27 \pm 0.08$ b
$\chi^2 = 12$ for 10 deg of freedom

TABLE XIII. Detailed summaries of analyses for individual nuclei. See caption of Table V.

Isotope $^{186}{}_{74}$W

Energies of lowest rotational states (keV)

$E(2^+)=122.6$
$E(4^+)=399$
$E(6^+)=820$

Parameters of deformed Fermi distribution

$r_0=1.132\pm0.004$ F	$c=6.459\pm0.023$ F
$a=0.478\pm0.012$ F	$t=2.100\pm0.053$ F
$\beta=0.222\pm0.002$	β (uniform) $=0.224$
$\rho_n=0.155$ F^{-3}	
$\langle r^2\rangle^{1/2}=5.373$ F	

Unperturbed energy levels (keV)	Quadrupole matrix elements (unrenormalized) (keV)
$1s_{1/2}=9185.277$	$2p$: $\alpha_{3/2,3/2}=40.51$
$2s_{1/2}=3013.873$	$\alpha_{3/2,1/2}=40.72$
$2p_{1/2}=3949.686$	$3d$: $\alpha_{5/2,5/2}=5.36$
$2p_{3/2}=3806.748$	$\alpha_{5/2,3/2}=5.43$
$3d_{3/2}=1760.091$	$\alpha_{3/2,3/2}=6.05$
$3d_{5/2}=1731.537$	

Observed transitions

	Energy (keV)		Intensity	
	Experiment	Theory	Experiment	Theory
K x rays	5182.12±0.37	5181.66	16.8±1.2	17.8
	5217.71±0.22	5217.85	35.9±1.2	32.1
	5286.02±0.40	5285.72	14.2±1.2	14.8
	5304.71±0.40	5304.26	10.7±1.0	11.5
	5407.79±0.32	5408.32	22.5±1.0	23.7
L x rays	2044.16±0.31	2044.94	37.1±2.8	36.8
	2148.74±0.34	2149.00	26.3±2.5	27.1
	2206.93±0.10	2206.83	36.6±0.8	36.1

$B(E2\colon 0^+\to2^+)=(3.55\pm0.20)\times10^{-48}$ cm^4 e^2
$Q(0,2)_{\mathrm{CE}}=5.93\pm0.05$ b
$Q(0,2)_\mu=5.90\pm0.08$ b
$\chi^2=29$ for 14 deg of freedom

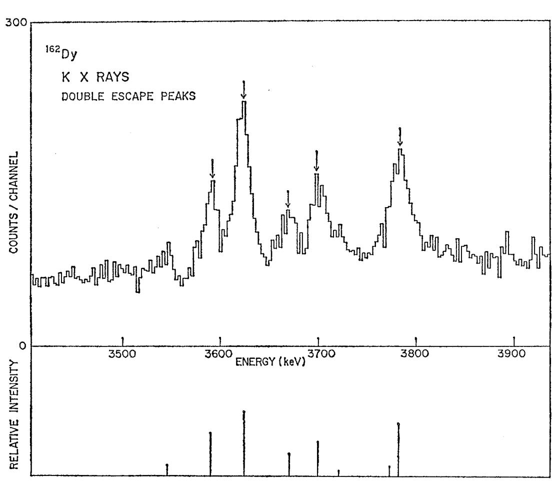

FIG. 10. K x rays of ^{162}Dy. Theoretical prediction shown underneath.

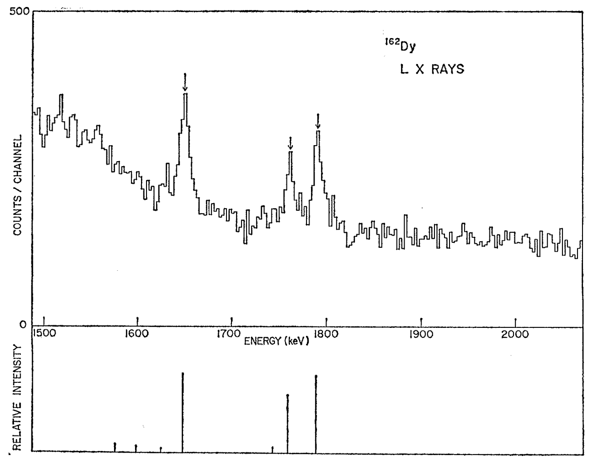

FIG. 11. L x rays of ^{162}Dy. Theoretical prediction shown underneath.

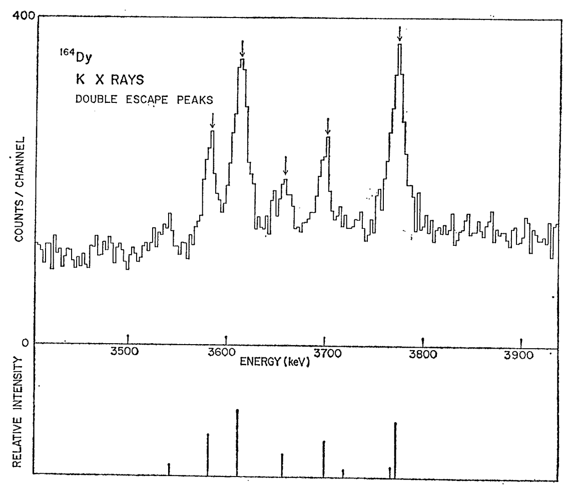

FIG. 12. K x rays of ^{164}Dy. Theoretical prediction shown underneath.

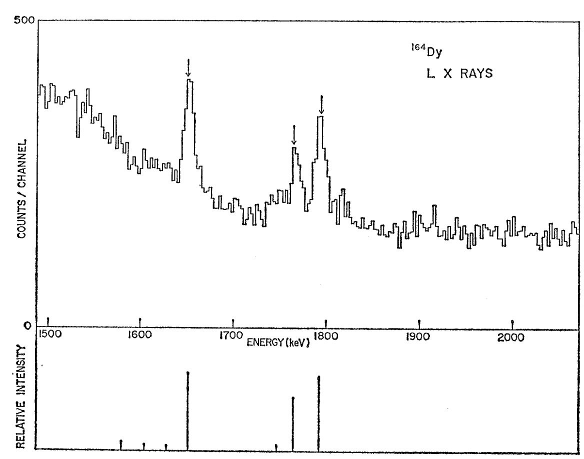

FIG. 13. L x rays of ^{164}Dy. Theoretical prediction shown underneath.

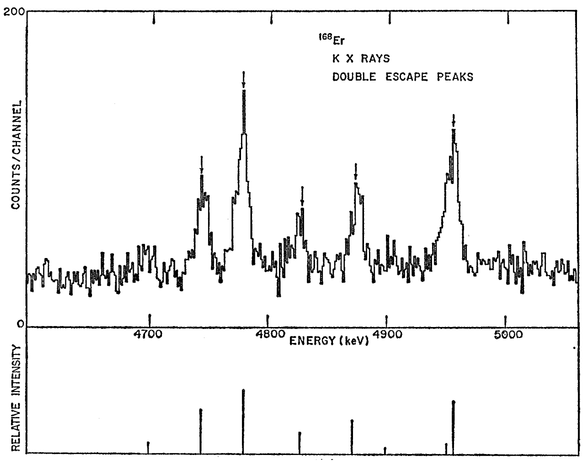

FIG. 14. K x rays of ^{168}Er. Theoretical prediction shown underneath.

precision of our determination of the parameters of the charge distribution.

A. $_{60}{}^{150}$Nd, $_{62}{}^{152}$Sm

These two nuclei occur at the sudden onset of large permanent quadrupole deformation at neutron number 90. Their rotational spectra are similar, although the energy levels of ^{152}Sm are known in greater detail. ^{152}Sm is also slightly more deformed than ^{150}Nd, as can be seen from its larger $B(E2:0^+\rightarrow 2^+)$ value. The isomer shifts of the 2^+ state of both nuclei have been

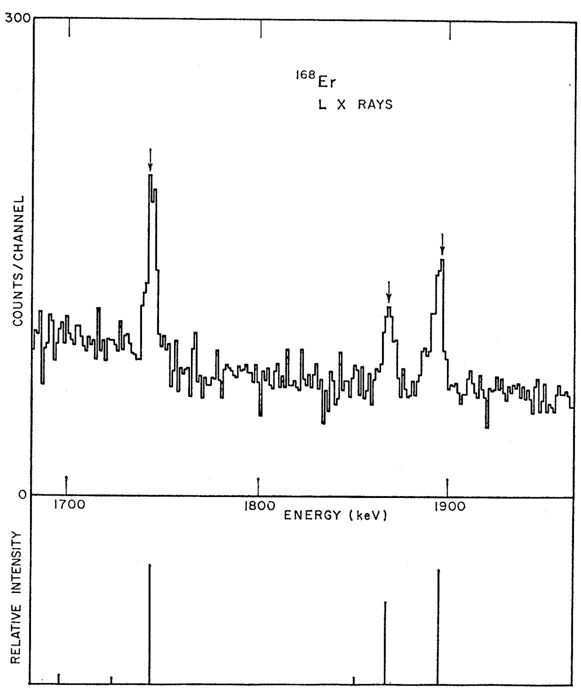

FIG. 15. L x rays of ^{168}Er. Theoretical prediction shown underneath.

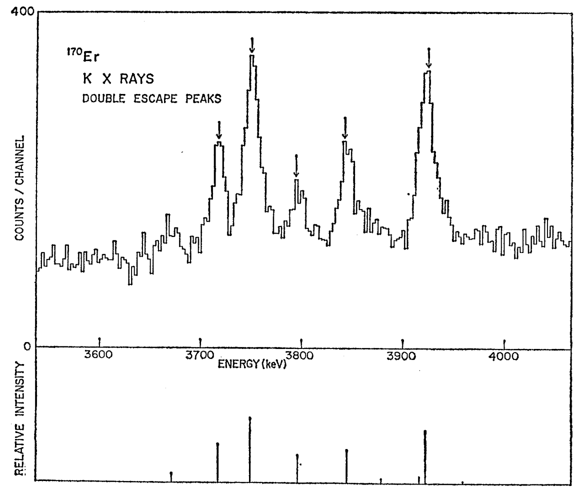

FIG. 16. K x rays of ^{170}Er. Theoretical prediction shown underneath.

measured[20] to be

$$\Delta\langle r^2\rangle^{1/2}/\langle r^2\rangle^{1/2}=5\times10^{-4}.$$

A good fit was obtained for the muonic x-ray spectra of both nuclei. The charge distributions are seen to be quite similar, except for the larger β of ^{152}Sm. In both cases, the Q_0 value is well reproduced. It is interesting to note that the addition of two protons causes the rms radius to increase more than the $A^{1/3}$ rule would predict. This isotone shift amounts to a shift in the 1s level energy of $\Delta E_{\text{obs}}=340.8$ keV, whereas for an equivalent uniform spherical distribution we would have $\Delta E_{\text{std}}=354.6$ keV, if the $A^{1/3}$ rule were followed. Note that the bulk of the level shift is due to the increase in Z.

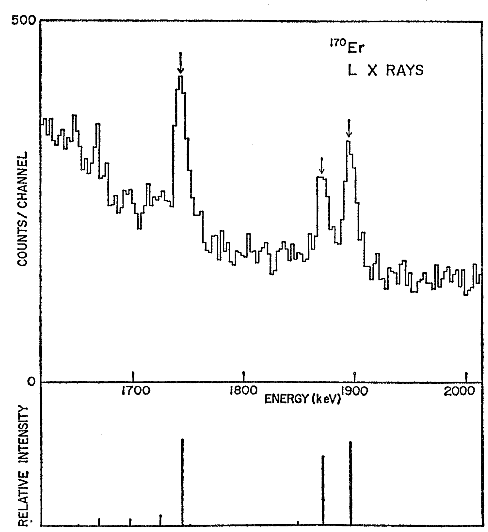

FIG. 17. L x rays of ^{170}Er. Theoretical prediction shown underneath.

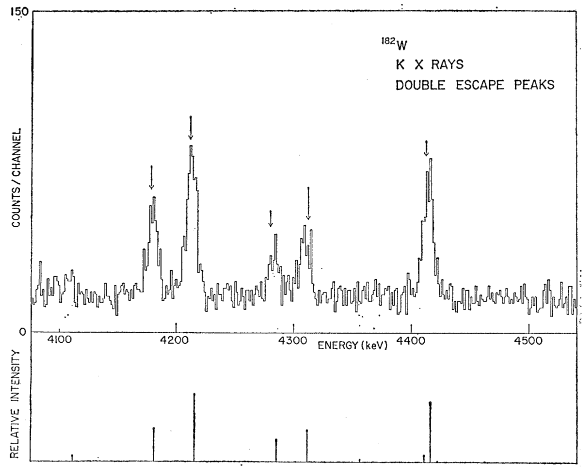

FIG. 18. *K* x rays of ^{182}W. Theoretical prediction shown underneath.

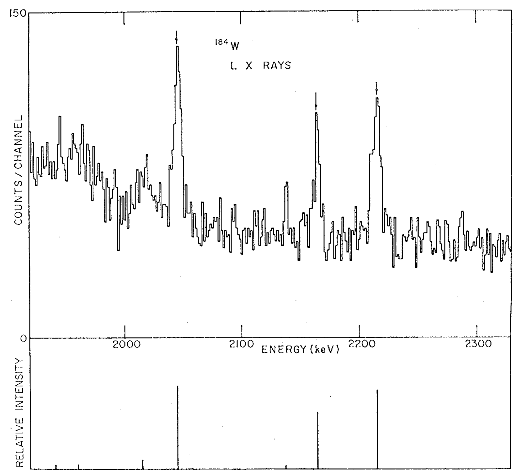

FIG. 21. *L* x rays of ^{184}W. Theoretical prediction shown underneath.

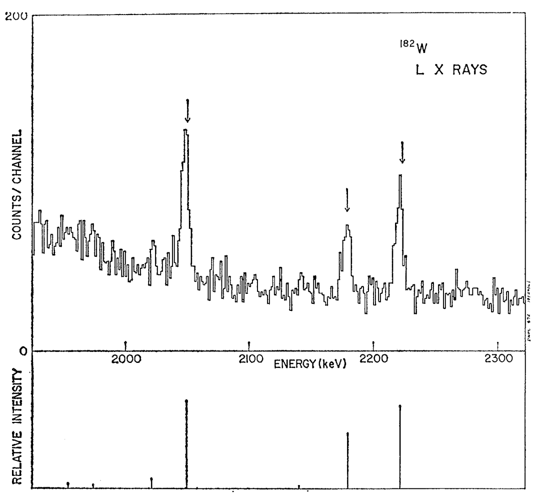

FIG. 19. L x rays of ^{182}W. Theoretical prediction shown underneath.

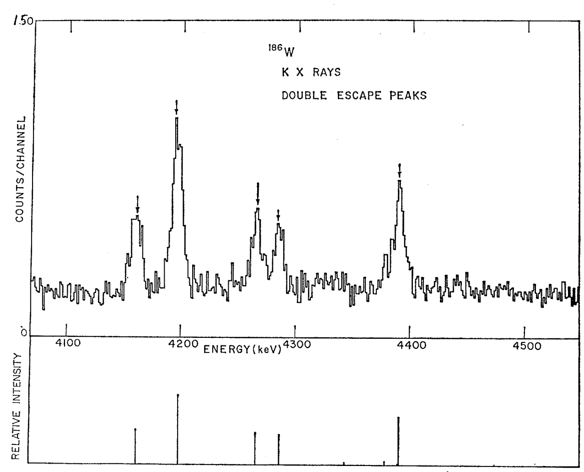

FIG. 22. *K* x rays of ^{186}W. Theoretical prediction shown underneath.

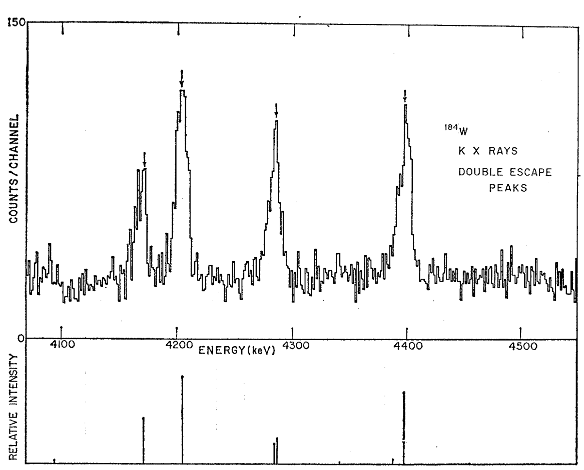

FIG. 20. *K* x rays of ^{184}W. Theoretical prediction shown underneath.

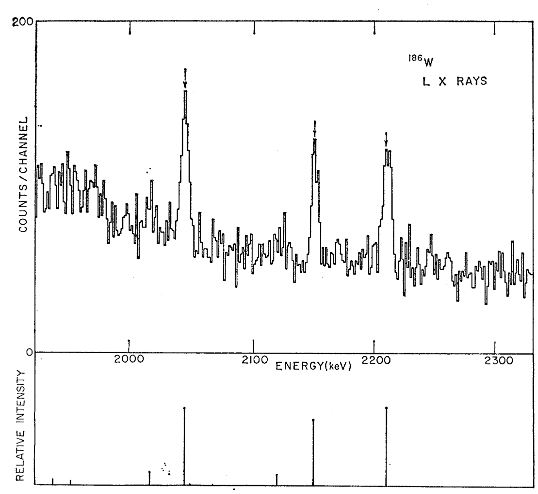

FIG. 23. L x rays of ^{186}W. Theoretical prediction shown underneath.

B. $_{66}{}^{162}$Dy, $_{66}{}^{164}$Dy

The two isotopes of Dy are highly deformed and show good rotational spectra, which, along with $B(E2\!:\!0^+\!\rightarrow\!2^+)$ measurements, indicate that ^{164}Dy is slightly more deformed than ^{162}Dy. No isomer shift measurements have been made for these nuclei, but only a very small shift would be expected.

The present analysis indicates that the charge distributions of these two nuclei are somewhat different. The skin thicknesses are 2.4 F for ^{162}Dy and 2.2 for ^{164}Dy. The deformation parameters are roughly the same, in contrast to the deformation parameters derived from the $B(E2\!:\!0^+\!\rightarrow\!2^+)$ values. This is reflected in the fact that our best fit $Q(0, 2)$ value for ^{162}Dy (7.36 ± 0.10 b) is somewhat larger than the Coulomb excitation value (7.12 ± 0.12 b) while the $Q(0, 2)$ value for ^{164}Dy (7.42 ± 0.10 b) is in good agreement (7.50 ± 0.20 b). The isotope shift in these two nuclei is smaller than would be expected from the $A^{1/3}$ rule. We find that

$$\Delta E_{\rm obs}/\Delta E_{\rm std}=10.0\pm0.5/21.0\ {\rm keV}=0.48\pm0.03.$$

The ratio of the measured electronic x rays to standard isotope shift for these two nuclei is 0.63 ± 0.05.[37]

C. $_{68}{}^{168}$Er, $_{68}{}^{170}$Er

These isotopes of Er are also highly deformed and have very similar rotational spectra. No isomer shift measurements have been made for these nuclei. The isomer shift for ^{166}Er, a very similar nucleus, has been found to be quite small.[20]

We find that a good fit can be obtained to the spectrum of ^{168}Er with a skin thickness of 2.18 F, while ^{170}Er gives a best fit for a value 1.94. This is the smallest value for the nine nuclei under discussion. The χ^2 of the fit to ^{168}Er is 64 for 14 deg of freedom, which is the worst χ^2 of the nine fits. It is due mostly to the poor fit to the intensities; the χ^2 contribution is $\chi^2(\text{intensities})=55$. The observed 1$s$ level shift is 8.4 ± 0.5 keV, whereas $\Delta E_{\rm std}=22.9$ keV, yielding $\Delta E_{\rm obs}/\Delta E_{\rm std}=0.37\pm0.03$.

D. ^{182}W, ^{184}W, ^{186}W

The even-even isotopes of tungsten are of particular interest for tests of the validity of the rotational model. They lie in a transition region in which the large permanent deformations of the rare-earth nuclei give way to increasingly more spherical equilibrium shapes. From ^{182}W to ^{184}Wto ^{186}W, the equilibrium deformations decrease [$\beta(\text{uniform})=0.252$, 0.236, 0.224], and the energy spectra of the lowest rotational band show increasing deviations from the $I(I+1)$ rule. In addition, the energies of the γ-band head ($I=2$, $K=2$) decrease from 1222 to 904 to 730 keV, indicating that the nuclei are becoming "softer" to γ vibrations and that the admixture of γ-band states into the ground-state rotational bands is increasing. Despite this evidence for a breakdown of the rotational model, the isomer shifts have been found to be quite small for all three nuclei.[20]

We find that the charge distributions of these nuclei are quite similar, and a good fit is obtained for all three. However, with the ratio $R=Q_0(2, 2)/Q_0(0, 2)$ fixed at 1.0, the χ^2 of the fit to ^{186}W is considerably worse than for the other isotopes. In order to test for a possible breakdown of the rotational model, we have allowed R to vary from unity as an additional free parameter in the search procedure. A significantly lower total χ^2(13.0 for 13 deg of freedom) was obtained with $R=0.98\pm0.03$. A small, but not very convincing deviation from the rotational model is thus indicated. The r_0, a, and β found for this R agree with the $R=1$ values within the experimental uncertainty. No deviation was found for ^{182}W or ^{184}W.

Kumar and Baranger[38] using a pairing plus quadrupole model have made predictions for the static and dynamic moments of isotopes of the transition elements tungsten, osmium, and platinum. Their predictions for tungsten are shown in Table XII.

A measurement by Persson, Blumberg, and Agresti[39] of the ratio of the quadrupole moments of the first

TABLE XIV. Comparison of the ratio $R=Q_0(2, 2)/Q_0(0, 2)$ as predicted by Kumar and Baranger (Ref. 38) and measured by Persson, Blumberg, and Agresti (Ref. 39), Chow *et al.* (Ref. 41), and in the present experiment.

	$\dfrac{Q_0(2,2)_{182}}{Q_0(0,2)_{182}}$	$\dfrac{Q_0(2,2)_{184}}{Q_0(0,2)_{184}}$	$\dfrac{Q_0(2,2)_{186}}{Q_0(0,2)_{186}}$
Rotational model	1.0	1.0	1.0
Kumar and Baranger[a]	1.0	1.0	0.91
Persson, Blumberg, and Agresti[b] and Persson and Stokstad[c]	1.0	0.99 ± 0.02	0.98 ± 0.02
Chow *et al.*[d] and Persson and Stokstad[c]	1.0	0.983 ± 0.019	1.005 ± 0.028
This experiment	1.0	1.00 ± 0.03	0.98 ± 0.03

[a] Reference 38.
[b] Reference 39.
[c] Reference 40.
[d] Reference 41.

[37] F. Boehm, Proceedings of the International Conference on Nuclear Structure, Dubna, 1968 (unpublished).

[38] K. Kumar and M. Baranger, Phys. Rev. Letters **17**, 1146 (1966).

[39] B. Persson, H. Blumberg, and D. Agresti, in Proceedings of the International Conference on Hyperfine Interactions Detected by Nuclear Radiation, Paper I.13, 1967 (unpublished).

TABLE XV. Isotope shifts in the W isotopes. The muonic results are compared with optical and electronic x-ray measurements. Optical results are not corrected for specific-mass effects.

Isotopes	Isotope shifts $(\Delta E)_{\text{obs}}$	$(\Delta E)_{\text{std}}$	$(\Delta E)_{\text{obs}}/(\Delta E)_{\text{std}}$ Present work	Optical	Electronic K x rays
182–184	9.52 ± 0.40	15.6	0.61 ± 0.03	0.45 ± 0.08	0.65 ± 0.08
184–186	7.24 ± 0.40	15.8	0.46 ± 0.03	0.40 ± 0.07	0.43 ± 0.06

excited states of the even-even isotopes (from the quadrupole broadening of the Mössbauer transition), when combined with the latest $B(E2\colon 0^+\rightarrow 2^+)$ measurements of Persson and Stokstad,[40] yields results which agree more closely with the rotational model than with the Kumar and Baranger result.

These findings are confirmed by a recent Columbia measurement of hyperfine Mössbauer spectrum in W in a single WS_2 crystal with C axis parallel or perpendicular to the incident γ radiation following Coulomb excitation.[41] These ratios, also combined with $B(E2)$ values, agree as well with the rotational model prediction. The results of all three determinations of R are also summarized in Table XIV.

A word is in order about the strengths and weaknesses of these determination of R. The Mössbauer measurements yield the ratios of the quadrupole moments of the first excited state of the three isotopes. What is measured is a product of the nuclear quadrupole moment and the electric field gradient at the nucleus caused by atomic electrons, which is assumed to be independent of the isotope and to depend only on the electronic configuration of a particular compound. In addition, in the experiment reported in Ref. 35, the crystal structure of the compound may be such that there is an asymmetric field gradient at the nucleus, and this asymmetry must be measured. The experiment of Chow *et al.*,[41] in which source and absorber are identical for all three isotopes, avoids this source of uncertainty. The $B(E2\colon 0^+\rightarrow 2^+)$ ratios are then introduced, and the ratios of the parameter R for the three isotopes are determined.

The muonic x-ray determination of R involves only a single isotope, and R may be obtained directly. However, the conclusion in this case is model-dependent, since it is the ratio of the product of the quadrupole moment times the form factor which is determined. Both methods, however, indicate that deviations from the rotational model in ^{186}W are slight.

In the case of the even-even tungsten isotopes, it is possible to compare the isotope shifts with both optical and electronic K x-ray measurements. It should be noted that the optical results are not corrected for the specific mass shift. The results are summarized in Table XV.

VI. CONCLUSION

The main purpose of studying the dynamic $E2$ hyperfine spectra is to obtain information about the charge distribution in both ground and excited states of deformed nuclei. In our several different attempts to interpret our experimental results, we have come to appreciate how sensitively the conclusion depend on the precision of the theoretical corrections which include the isomer shift, Lamb shift, and most important but less certain, the nuclear polarization corrections. The definition of nuclear polarization applies to any perturbations which induce mixing between the excited states and the ground state. Therefore the dynamic $E2$ hyperfine spectra could also be considered as the manifestation of the nuclear polarization due to the quadrupole interaction. However, in the original calculations of this effect, the quadrupole interaction H_Q was diagonalized between the "model space" states only [i.e., between the doublets $(2p_{3/2}, 2p_{1/2})$, $(3d_{5/2}, 3d_{3/2})$ and the lowest rotational band of the nucleus]. In reality, the electrostatic interaction connects all possible states, both bound and continuum muon states and nuclear states outside the lowest rotational band. In a precise analysis of the dynamic $E2$ hyperfine spectra, the nuclear polarization correction must be calculated to include all states beyond the "model space." To illustrate the dependence of our conclusions on the precision of the nuclear polarization correction, we have listed in Table XVI the results of the best fits to the ^{182}W data obtained with corrections including all states as calculated by Chen and those including only states within the model space. For historical reasons and also for brevity, we have called the former "with corrections" or "renormalized" and the latter "corrections not included." Perhaps the most unsatisfactory feature of the results without correction (column II) is the very small skin thickness (1.736 F) obtained. In addition, the quadrupole moment value ($Q=6.71$ b) was larger than that derived from Coulomb excitation ($Q=6.58$ b).

[40] B. Persson and R. G. Stokstad, Bull. Am. Phys. Soc. **12**, 1124 (1967).

[41] Y. W. Chow, E. S. Greenbaum, R. H. Howes, F. H. H. Hsu, P. H. Swerdlow, and C. S. Wu, Bull. Am. Phys. Soc. **14**, 556 (1969); and (to be published).

Finally, it was not possible in this analysis to obtain a reasonable interpretation of the relative intensities of the K and L x rays.

Before the improved nuclear polarization corrections were made, another approach was attempted to reduce the quadrupole moment value in order to bring it into agreement with that obtained from Coulomb excitation. This is to allow the skin thickness to vary with polar angle: $a' \to a(1+\beta' Y_{20})$. The results of this four-parameter fit (c, a, β, and β') are shown in column III. A best fit was obtained for all nuclei with rather large negative values for the β' parameter, implying that the nuclear charge distribution was more diffuse at the "equator" ($\theta=90°$) than at the "poles" ($\theta=0°$). For ^{182}W, the main effect of the introduction of the fourth parameter was to provide a good fit to the Q_0 value. The skin-thickness parameter was increased only slightly, while the χ^2 of the fit to the intensities did not improve.

The best-fit parameters shown in column I are obtained with the "renormalized" nuclear polarization corrections. It will be noted that the skin thickness of the three-parameter distribution is 2.12 F, a value similar to that obtained for neighboring nuclei. The inclusion of the nuclear polarization correction to the $2p$ levels (refer to Table I and Fig. 4 of Ref. 13) is responsible for this increase in skin thickness. In addition, the renormalization of the quadrupole interaction, through the use of H_{eff}, has made it possible to obtain a good fit to the energy splittings with a quadrupole moment which agrees with the Coulomb excitation result. The modification of the $E1$ matrix elements through inclusion of the polarization corrections has also made it possible to obtain a more reasonable χ^2 for the fit to the relative intensities of the x rays.

The great improvements of the best fits were found in all the nine deformed nuclei which we investigated as shown in Table IV. While this general agreement speaks strongly for the adequacy of a three-parameter deformed Fermi distribution, it should be borne in mind that it does not imply that the nuclear charge distribution is precisely as described by the model. It does suggest that more complicated models are not, here, justified. Of the three parameter models the one used is certainly among the most simple.

TABLE XVI. Comparison of best-fit parameters for $^{182}_{74}$W with and without inclusion of nuclear polarization and Lamb-shift corrections. The possibility of a skin thickness which varies with polar angle is allowed in column III, where the replacement $a \to a(1+\beta' Y_{20})$ is made. The value of Q_0 from $B(E2)$ measurements is 6.58 b.

	I Corrections included 3-parameter model	II Corrections not included 3-parameter model	III Corrections not included 4-parameter model
c	6.409±0.023 F	6.510	6.471
t	2.118±0.053 F	1.736	1.852
β	0.248±0.002 F	0.250	0.272
β'	≡0	≡0	−0.51
Q_0	6.57±0.08 b	6.71	6.57
χ^2 (energy)	1.9	6.5	6.6
χ^2 (intensity)	9.3	29.0	26.8

ACKNOWLEDGMENTS

The authors wish to thank Dr. G. L. Rogosa of the U. S. Atomic Energy Commission for his cooperation in making the separated isotopes available to us for this investigation. We are also indebted to Dr. K. Runge who contributed greatly to the investigation at the early stage of the work. We are also grateful to W. Patton for his contribution to the programming of the on-line computer, and to Marco Cirincion for his assistance in procuring the targets.

The electronics used in the experiment were designed and built by our electronic group under the guidance of J. Hahn, V. Guiragossian, M. Konrad, T. Becker, and R. Bondurant. Our sincere appreciation goes to Dr. M. Y. Chen whose calculations on the high-order nuclear-polarization corrections and whose concise and lucid explanation contributed greatly to the understanding of our results. We also wish to thank W. Y. Lee for his contribution during the course of the experiment.